

Synthesis, charge transport studies, and microwave shielding behavior of nanocomposites of polyaniline with Ti-doped γ -Fe₂O₃

S. Anoop Kumar · Avanish Pratap Singh ·
Parveen Saini · Fehmeeda Khatoon ·
S. K. Dhawan

Received: 15 June 2011 / Accepted: 19 October 2011 / Published online: 8 November 2011
© Springer Science+Business Media, LLC 2011

Abstract This article reports the synthesis, charge transport studies, and microwave shielding properties of polyaniline–Ti-doped γ -Fe₂O₃ nanocomposite. The composite has been prepared by the in situ chemical oxidative polymerization using dodecylbenzenesulfonic acid as a dopant. These resulting polymer composites have been found thermally stability up to 260 °C with magnetization value of ~ 10 emu/g. The temperature dependence of electrical conductivity reveals the applicability of Mott's 3D-VRH model. The composites has shown the shielding effectiveness of 35.64–45.20 dB (>99.99% attenuation) in 12.4–18 GHz (Ku-Band) frequency range. The enhancement of SE has been due to combination of dielectric and magnetic losses leading to decrease in skin depth increase in total (σ_T) conductivity and better matching of input impedance.

Introduction

Electromagnetic (EM) shielding represents a way toward the improvement of the electromagnetic compatibility (EMC). It attracts great attention because of wide and

extensive use of electronic equipments like cellular phones, Television, radar etc. that operates in the microwave band. An unnecessary interruption emitted from an external source carrying transient currents from these instruments called electromagnetic interference (EMI) and it severely affect the life and performance of the electrical circuit due to electromagnetic (EM) radiation [1, 2]. Therefore some protection mechanism must be provided to guard these equipments from harmful effect of these EM noises. For the commercial applications material with shielding effectiveness (SE) greater than 30 dB is sufficient, while for defense application, the requirement are significantly higher i.e. between 80 and 100 dB. The enhancement of microwave absorption comes mainly from the combination of magnetic and dielectric losses as well as moderate conductivity of the shield material. At high frequency, the permeability of the magnetic material decreases due to the eddy current losses developed by the EM wave. Therefore, it is better to use conducting polymer matrix to suppress the eddy current phenomenon to enhance the effective interaction with the absorber. Intrinsic conducting polymers (ICPs) having extended π -conjugated system with conductivity in semiconductor regime has emerged as a potential class of materials for EMI shielding and microwave absorbers [3–7]. Many research groups are working on this aspect of conjugated polymers, as unlike metals, they not only reflect the EM radiation but also absorb them. The properties of conducting polymer (polyaniline) not only depend on the oxidation state but also on its protonation state/doping level and also on the nature of dopants. Polyaniline (PANI) demonstrates a distinctive feature in the sense that it is not charge conjugation symmetric, i.e., the valence and conduction bands are asymmetric to a great extent. As a result, the energy level positions of doping-induced absorptions differ widely from those of the charge

Electronic supplementary material The online version of this article (doi:10.1007/s10853-011-6068-5) contains supplementary material, which is available to authorized users.

S. Anoop Kumar · A. P. Singh · P. Saini · S. K. Dhawan (✉)
Polymeric & Soft Materials Section, National Physical
Laboratory (CSIR), Dr. K. S. Krishnan Road,
New Delhi 110 012, India
e-mail: skdhawan@mail.nplindia.ernet.in

S. Anoop Kumar · F. Khatoon
Department of Applied Sciences, Faculty of Engineering &
Technology, Jamia Millia Islamia, New Delhi 110025, India

conjugation symmetric polymers [8]. Studies on the above aspect and also on temperature dependence of conductivity and transport mechanism have also generated a prominent interest.

Recently, several interesting research projects have focused on the preparation of PANI with ferromagnetic properties, such as oxide, sulfide, nitride, metal, and clay materials [9, 10]. Much work has been done on γ -Fe₂O₃, Fe₃O₄, BaTiO₃, and TiO₂ in the field of EM wave adsorbing. In our earlier study, carried out in our laboratory, nanoparticles of γ -Fe₂O₃, TiO₂ were added separately in the polymer matrix in which γ -Fe₂O₃ act as magnetic filler and TiO₂ act as dielectric filler. The SE due to absorption part for PANI- γ -Fe₂O₃, PANI-TiO₂, PANI-TiO₂- γ -Fe₂O₃ composite, respectively, are 8.8, 22.4, and 45 dB. The PANI, PANI- γ -Fe₂O₃ composite shows one dimensional VRH model whereas incorporation of TiO₂ nanoparticle in PANI- γ -Fe₂O₃ matrix change the dimension of the conductivity from one dimensional to three dimensional. The incorporation of γ -Fe₂O₃ and TiO₂ in polymer matrix introduces heterogeneity in the composites with difficulty in controlling the EM attributes. In this study, we have synthesised Ti-doped γ -Fe₂O₃ (FT) to introduce magnetic as well as dielectric properties within single filler. These FT nanoparticles have been encapsulated inside PANI matrix by in situ emulsion polymerization and its effect on the electrical, thermal, spectral, and EM properties of PANI has been studied. We achieve nearly similar result of SE value by using less amount of filler from our previous study. In the previous study, we have used more filler [PANI: TiO₂: γ -Fe₂O₃ :: 1:1:2 i.e. is polymer to filler ratio 1:3], but in this article we have used [PANI:Ti-doped- γ -Fe₂O₃ :: 1:2]. The dielectric and magnetic contribution of FT and finite conductivity of PANI results in effective attenuation of microwave radiations and can find application in high performance absorbing material [11–16].

Experimental

Materials

Aniline (Loba Chemie, India) has been freshly distilled before use. Dodecylbenzene sulfonic acid (DBSA), ammonium peroxydisulfate (APS, Merck, India), isopropyl alcohol (Merck, India), ferric chloride (FeCl₃ Merck, India) and ferrous chloride (FeCl₂·4H₂O Merck, India) and titanium chloride (TiCl₄ Merck, India) and chloroform (Qualigens, India) have been used as received. FT nanoparticles have been synthesised by chemical co-precipitation method. Aqueous solutions have been prepared from the double distilled water having conductivity of 10⁻⁶ ohm⁻¹ cm⁻¹.

Synthesis of the nano crystalline titanium-doped γ -ferric oxide (FT)

The FT has been prepared through the conventional co-precipitation method [17]. A mixture of anhydrous ferric chloride (FeCl₃), ferrous chloride (FeCl₂·4H₂O) along with titanium chloride (TiCl₄) in molar ratio of 1.28:0.65:0.07 have been prepared in a glove box. The resulting solution has been precipitated by adding 1 M aqueous solution of ammonia drop by drop with continuous vigorous stirring for 5–7 h at room temperature, maintaining the pH of the solution at 9–10. The brownish black precipitate so formed has been filtered out and washed thoroughly with distilled water. The product so obtained has been dried for 24 h at 262 °C.

Polymer preparation

Synthesis of polyaniline (PANI)

The doped PANI has been prepared by chemical oxidative polymerization following direct approach and using DBSA as a surfactant dopant. 0.1 mol of aniline and 0.3 mol DBSA have been mixed in distilled water. The mixture has been homogenized using high speed blender rotating at 10,800 rpm for 30 min to form an emulsion. The so-formed emulsion solution has been transferred to double walled glass reactor and cooled to -5.0 °C under constant stirring. The polymerization has been initiated by the drop-by-drop addition of ammonium peroxydisulfate (APS) (0.1 mol), (NH₄)₂S₂O₈) in 100 mL distilled water and the temperature has been maintained at -5.0 ± 1.0 °C. After complete polymerization a dark green emulsion has been obtained. The emulsion obtained has been demulsified using equal amount of isopropyl alcohol and stirring has been continued for another 2 h after which the reaction mixture has been filtered to separate the polymer. The wet polymer cake has been dried under vacuum till constant rate at 50 °C and then crushed to obtain the powder of polyaniline (FPT0).

Synthesis of polyaniline composites (PANI-FT composites)

The composites have been also prepared by emulsion polymerization. For this purpose the calculated amount of FT powder has been added in 0.3 mol of DBSA have been mixed using high speed mixer with 500 mL of distilled water. Then 0.1 mol of aniline have been added in the above mixture and homogenized further to form stable emulsion. The resulting emulsion has been polymerized by ammonium peroxydisulfate (APS) under same conditions as for pure PANI (FPT0). Finally the powdered composites

have been obtained by filtration and drying. The different compositions containing 1:1 and 1:2 weight ratio of aniline to FT have been prepared and designated as FPT1, FPT2, respectively.

Characterization

Morphologies have been observed using transmission electron microscopy (TEM, JEOL JEM 1011) and the samples have been deposited on carbon-coated copper grids. The samples have been also studied by UV–Visible (Shimadzu UV-1601), and XRD studies have been carried out on D8 Advance Bruker AXS X-ray diffractometer from $2\theta = 20^\circ$ to 70° at a scan rate of 0.0258 s^{-1} . Thermogravimetric analyzer (Mettler Toledo TGA/SDTA 851 $^\circ$) has been used to measure the thermal stability of the material under inert atmosphere in the temperature range 25–800 $^\circ\text{C}$. The magnetic measurements of the ferrite as well as conducting composite have been carried out using vibrating sample magnetometer (VSM), Model 7304, Lakeshore Cryotronics Inc., USA. Pressed pellets (length 13 mm, width 7 mm, thickness ~ 2.7 mm) have been prepared and the low temperature conductivities have been measured by four-point probe technique using (Keithley 220 Programmable Current Source and 181 Nanovoltmeter). EMI SE values have been measured by placing rectangular pellets (~ 2.7 mm thick) inside

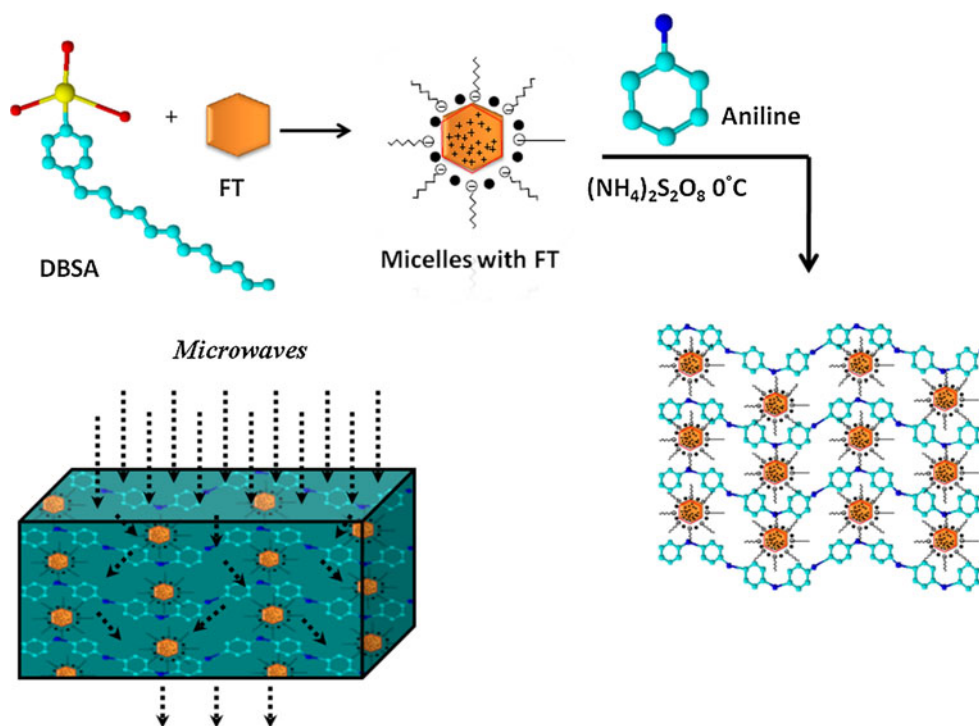
Ku-band (12.4–18 GHz) waveguides and using a Vector Network Analyzer (VNA E8263B Agilent Technologies).

Result and discussion

Mechanism

The PANI–FT composites have been prepared by in situ emulsion polymerization where aniline–FT mixture forms the dispersed phase and water acts as continuous phase. Due to the presence of polar– SO_3H head and nonpolar hydrophobic tail, DBSA acts as surfactant as well as dopant. Therefore, aniline–DBSA micelles acts as a soft template with formation of oil in water type emulsion. The addition of water soluble oxidant, i.e., APS initiates the polymerization reaction, which starts from the surface of the micelles and then propagates inside the bulk of the aniline dissolved in the micellar phase. The oxidation of monomer aniline leads to formation of anilinium radical cations which on combination with another unit form neutral dimer molecule. Further oxidation of this dimer and subsequent addition of monomer unit leads to the formation of a trimer, tetramer, and finally the conducting polymer, i.e., PANI. The schematic representation of PANI growth in FT matrix is shown in Scheme 1.

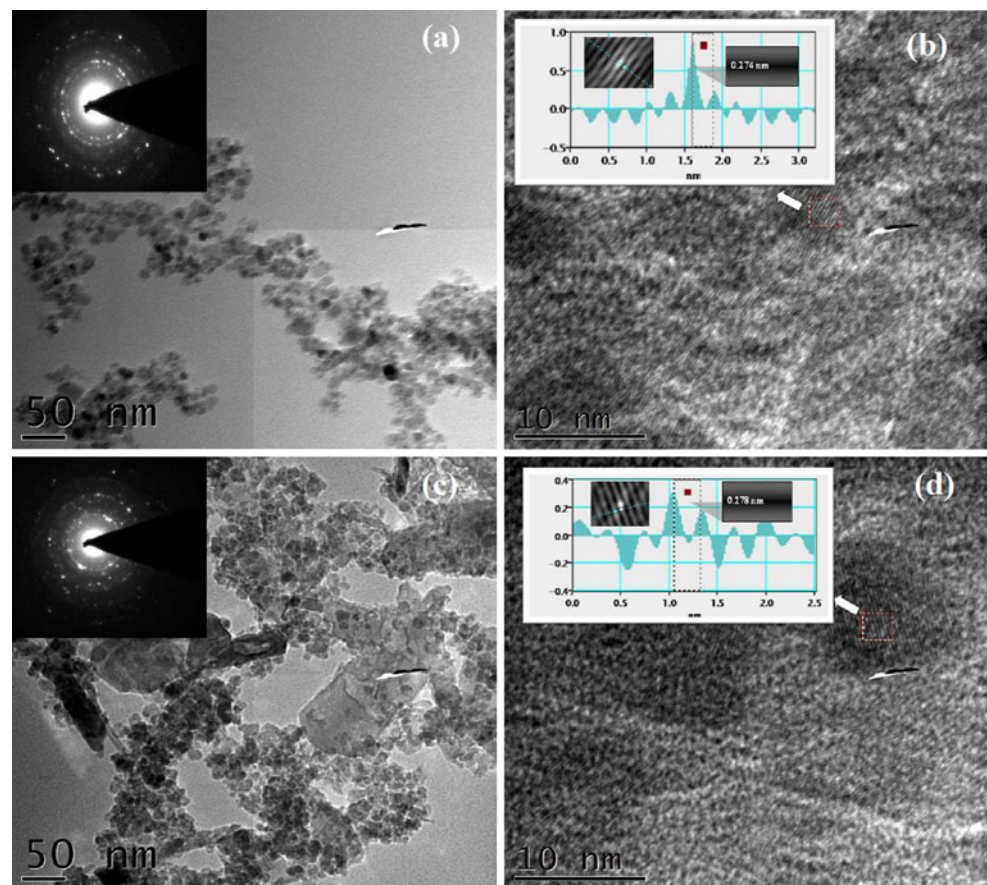
Scheme 1 Schematic representation of **a** polymerization of aniline containing the FT particles using APS as oxidant in the presence of DBSA leads to formation of polyaniline and **b** the interaction of the microwave with the polymer composite resulting in attenuation due to scattering with the FT particles



The morphological studies

The morphology and particle size of samples have been investigated by high resolution transmission electron microscopy (HRTEM). Figure 1 shows the TEM and HRTEM images of FT and PANI–FT nanocomposite, respectively. The Fig. 1a shows agglomerated FT particles with size in range of 8–10 nm, whereas the inset shows the electron diffraction patterns with characteristic radial distance corresponding to hexagonal FT. Figure 1c shows that FT particles have been coated with PANI with particle size in the range of 9–15 nm. The decrease in the intensity of diffraction dots (inset Fig. 1c) confirms the coating of crystalline FT nanoparticles with amorphous PANI shell. Figure 1b, d shows the HR-TEM images of FT and FPT2, respectively, showing lattice fringes (and lattice profile) with interplanar spacing (2.74 Å) corresponding to (112) planes of FT. These results matches with the d -value (2.74 Å) observed in the XRD patterns. The ferrite particles or their aggregates (dark area) are surrounded with PANI, and it can be considered that the FT has been coated by PANI with a core–shell structure.

Fig. 1 a and c shows the TEM image, whereas the *inset* shows electron diffraction patterns of FT nanoparticles and PANI–FT composite b and c shows the HRTEM image, whereas the *inset* shows lattice fringes (and lattice profile) with interplanar d -spacing of 0.274 and 0.278 nm for FT nanoparticles and PANI–FT composite, respectively



X-ray diffraction analysis

Figure 2 shows the X-ray diffraction patterns of FT, PANI, and their composites. The main peaks of FT are observed at 2θ values of 23.90° ($d = 3.71 \text{ \AA}$), 32.62° ($d = 2.74 \text{ \AA}$), 35.36° ($d = 2.53 \text{ \AA}$), 40.36° ($d = 2.23 \text{ \AA}$). On the other hand, diffractogram of PANI gives characteristic broad peaks at 2θ values of 25.14 , 35.81 , and 62.87° . It has been observed that, main peaks present in FT have been also observed in all the PANI–FT composites (i.e., FPT1 and FPT2), which indicates the presence of ferrite particles in the polymer matrix. The intensity of peaks increase with the increase in the ratio of FT indicating increased incorporation within PANI matrix.

Thermogravimetric analysis

Figure 3 shows the thermo-gravimetric curves (TG) of pure FT, PANI, and their composites. The materials have been heated from 25 to 800°C under a constant heating rate of $10^\circ\text{C}/\text{min}$ and in the inert atmosphere of nitrogen gas ($60 \text{ mL}/\text{min}$). The pure FT has excellent thermal stability up to 800°C and weight loss has been only 4.3%. In

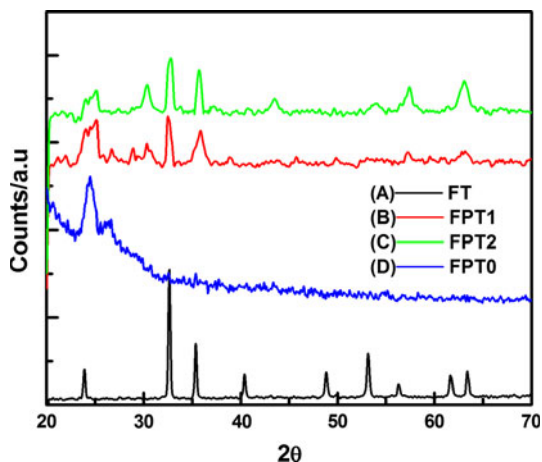


Fig. 2 X-ray diffraction patterns of plots of FT, FPT0, FPT1, and FPT2

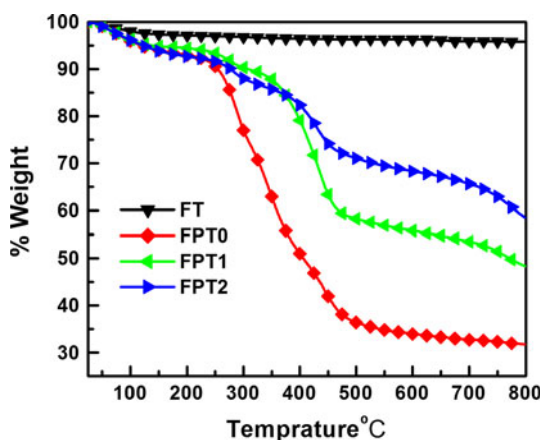


Fig. 3 Thermal gravimetric analysis of FT, polyaniline doped with DBSA and polyaniline composite with FT with increasing content FPT1, FPT2

composites, the first loss at 110 °C may be attributed to the loss of water and other volatiles. The weight loss in the second step, i.e., ~230 °C involves the loss of sulfonic (–SO₃H) part of the DBSA as well as onset of degradation of PANI backbone. The increasing FT content slightly affects the decomposition temperature (DT) which increases from 230 °C (FPT0) to 260 °C (FPT2). The third weight loss step between 250 and 550 °C can be ascribed to the complete degradation of dopant as well as polymeric backbone. The composites show little weight loss between the 500 and 800 °C and the residue remaining in this region gives an approximate estimate of filler content. Therefore, the % of FT actually incorporated into the system has been calculated and reported in Table 1. The results indicate that actually incorporated FT fraction is less than the ratio of aniline: FT taken in the initial reaction mass. The TGA data

clarify that these composites are thermally stability up to 260 °C, which envisages them as a good candidate for melt blending with conventional thermoplastics like polyethylene, polypropylene, polystyrene, etc.

UV–visible studies

Figure 4 shows the UV absorption spectra of the different samples of PANI and its composite with FT. The band around 363 nm is related to the π–π* transition whereas bands around 437 nm (polaron–π*) and 745 nm (π–polaron) are the characteristics of polarons. But in case of PANI composite, two changes have been observed. First a blue shift has been observed for the band from 745 to 734 and 730 nm for FPT1 and FPT2, respectively. Secondly, when the ratio of FT content increases in different samples, absorption spectra show the blue shift for the band 363 to 355 and 350 nm. The reason behind this shifting may indicate that the interaction appears between FT particles and PANI backbone, which may make the energy of anti-bonding orbital to increase [18], leading to the energy of the π–π* and (π-polaron) transition of the benzenoid and quinoid ring to increase, and consequently the absorption peaks of composite exhibit a blue shift. The optical band energy of the polymer has been obtained from the given relation [19]:

$$\alpha hv = A (hv - E_g)^{1/2} \tag{1}$$

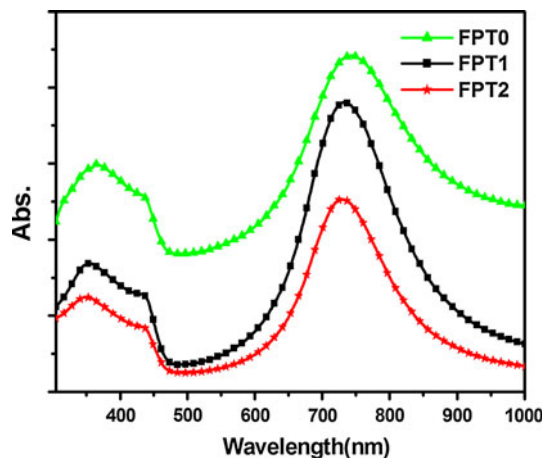
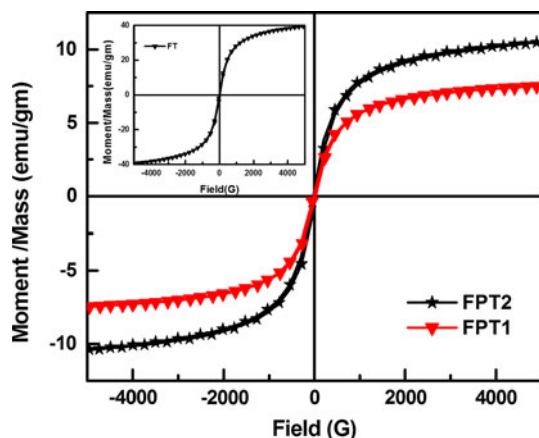
where α is the absorption coefficient, hv is the photon energy, and E_g is the optical band gap. The band gaps calculated by using the Eq. 1 are reported in Table 1. The band gap is calculated by the slope of curve between hv and (αhv)² (see supporting document Fig. 1) and data shows that as the amount of FT increases, the band gap increases.

Magnetic properties

Figure 5 shows the room temperature magnetization behavior of PANI–FT nanocomposites, whereas inset shows the hysteresis loop of pure FT. The saturation magnetization (M_s) values have been reported in Table 1. The negligible retentivity (M_r) and coercivity (H_c) of the materials indicate the super-paramagnetic behavior of these nanocomposites, which can be attributed to the small size of the FT particles, i.e., approaching the single domain limit. The conducting coating of PANI over FT nanoparticles affects the surface electron density, and hence the spin–spin or spin–lattice couplings. This is again manifested in terms of enhancement of relaxation rate of magnetic domains. The M_s value decreases with increasing PANI due to its nonmagnetic character. A systematic decrease in M_s and related increase in H_c for composite has

Table 1 Initial decomposition temperature (IDT), shielding effectiveness, magnetic saturation value (Ms), and band gap of PANI–FT composites

Sample Name	FT content (wt%)		IDT (°C)	UV–Vis peak(nm)	Band gap (eV)		Ms (emu/gm)	EMI SE _T Max of powder sample(dB)
	Initial % in reaction mixture	Calculate from char residue in TGA			π - π^*	π -polaron		
FT	100	–	700				39.372	–
FPT0	0	0	230	363,438,745	2.26	1.30	–	23.66
FPT 1	50	18	247	355,437,734	2.3	1.43	7	35.6
FPT 2	66	27	260	350,435,730	2.49	1.44	10	45.2

**Fig. 4** UV–Visible spectra of PANI–FT composites with different FT contents**Fig. 5** Magnetization curves of FT, FPT1, FPT2 showing the decrease in saturation magnetization with the decrease in FT content

been also observed. The coercivity of PANI–FT composite in this study presents a higher value than that of pure FT. It is known that the coercivity is related to the microstructure, magnetic anisotropy (crystal, stress, and shape), and magneto restriction of magnetic ferrite particles. The

anisotropy and magneto restriction are dependent on factors like composition, imperfections, porosity, crystalline shape, etc.

Polycrystalline ferrites have an irregular structure, geometric, and crystallographic nature, such as pores, cracks, surface roughness, and impurities. In the polymerization process, PANI is deposited on the ferrite surface and crystallite boundary, which may lead to an increase in magnetic surface anisotropy of ferrite particles. On the other hand, there is a possible charge transfer between the ferrite surface and PANI chains. This interaction may change the electron density at the ferrite surfaces and thus, affect the processes of electron spins in the system, resulting in the increase of spin–orbit couplings at the surface of ferrite particles [18].

Conductivity measurement

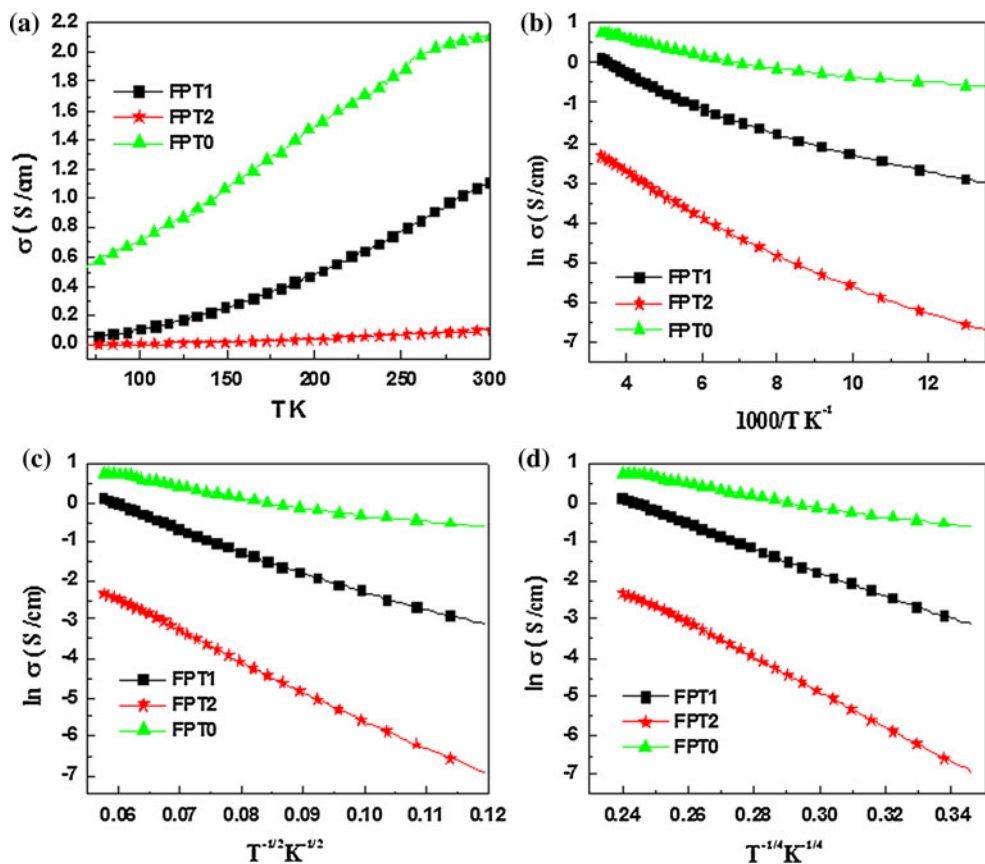
To investigate the charge transport mechanism, the temperature-dependent DC conductivity of the PANI–FT composite having different weight ratio of FT contents have been measured at temperature ranging from 70 to 300 K. The tunneling contribution to conductivity is dominant only at very low temperatures (below 70 K). The conductivity follows a typical semiconducting behavior showing decrease in value with the decreasing temperature. The room temperature conductivity of the samples is shown in Table 2. Figure 6a shows the conductivity decreases with the increase in weight fraction of FT phase which is ascribed to the insulating nature ($\sigma \sim 10^{-8}$ S/cm) of the FT particles. The particles cause carrier scattering leading to partial blockage of conduction path. Further the incorporation of FT particles between the chains also reduces the interchain coupling.

Several models have been used to explain the conductivity behavior in polymer like Arrhenius law and Mott's equation. In the Arrhenius model, conduction is related to excited carriers beyond the mobility edge into the non-localized or extended states and temperature-dependent conductivity can be expressed as [20]:

Table 2 DC conductivity, activation energy and Mott’s parameters of PANI–FT composite

Sample	σ (S/cm)	σ_0 (S/cm)	T_0 (K)	$N(E_F)$ (ev ⁻¹ cm ⁻³)	R_{hop} (Å)	W_{hop} (ev)	R/L
FPT0	2.11	67.13	42055.29	1.85×10^{23}	3.87	0.022	1.29
FPT1	1.11	2015.55	963450.44	8.08×10^{21}	8.47	0.049	2.82
FPT2	0.09	4504.22	3851231.38	2.02×10^{21}	11.98	0.069	3.99

Fig. 6 Variation of conductivity (σ) as a function of temperature in the range from 300 to 70 K for PANI–FT composites. **b** $\ln\sigma$ versus $1000/T$ **c** $\ln\sigma$ versus $T^{-1/2}$ **d** $\ln\sigma$ versus $T^{-1/4}$



$$\sigma(T) = \sigma_0 \exp \left[-\frac{E_a}{k_B T} \right] \tag{2}$$

where σ_0 is the proportionality constant, E_a the activation energy, k_B the Boltzmann constant, and T is the Kelvin temperature.

On the other hand, under Mott’s variable range hopping (VRH) regime conductivity can be best expressed by following equation [21, 22]:

$$\sigma(T) = \sigma_0 \exp \left[-\left(\frac{T_0}{T} \right)^\gamma \right] \tag{3}$$

where σ_0 is the conductivity at $T = \infty$ and T_0 is the characteristic Mott temperature. Exponent ‘ γ ’ in Eq. 3 is the dimensionality factor having values 1/2, 1/3, and 1/4 for 1, 2, and 3 conduction mechanisms, respectively.

Figure 6b shows that the plots of $\ln\sigma$ versus $1000/T$ have been linear only in high temperature region and fits poorly

at low temperatures, indicating the inapplicability of Arrhenius model. However, when plotted under Mott’s regime all samples show linearity with various fit parameters. It has been observed in Fig. 6c that linearity factors for $\ln\sigma$ versus $T^{-1/2}$ have been 0.9968 and 0.9994 for FPT1 and FPT2, respectively. However, when plotted as $\ln\sigma$ versus $T^{-1/4}$, fit factors have been found to be 0.9995 and 0.9996 for the FPT1, and FPT2, respectively, Fig. 6d. These values have been quite near to each other making the choice of transport system extremely difficult task. In order to resolve the above discrepancy and select the proper transport system, we have measured the slopes (which represents exponent ‘ γ ’) of log–log plots between reduced activation energy [23] and temperature (see supporting document Fig. 3). The straight line corresponding to $\gamma = 2$ indicate that the VRH mechanism of type $T^{-1/4}$ (i.e., 3D-VRH) explains the conduction mechanism in the polymer composites. As you see from our previous study PANI,

PANI- γ -Fe₂O₃ composite shows one-dimensional VRH model, whereas incorporation of TiO₂ nanoparticle in PANI- γ -Fe₂O₃ matrix change the dimension of the conductivity from one dimensional to three dimensional, similar behavior shown by PANI-FT nanocomposite.

For variable-range hopping in three dimensions (3D-VRH), the temperature dependence of conductivity follows the relation:

$$\sigma(T) = \sigma_0 \exp \left[- \left(\frac{T_0}{T} \right)^{1/4} \right] \quad (4)$$

The characteristic Mott temperature for 3D-VRH is given by:

$$T_0 = \left[\frac{18.1}{k_B N(E_F) L^3} \right] \quad (5)$$

where L is the localization length, k_B is the Boltzmann constant, $N(E_F)$ is the density of states at the Fermi energy. The range of hopping (R_{hop}) between two localized state and activation energy (W_{hop}) are expressed as

$$R_{\text{hop}} = \left[\frac{9L}{8\pi k_B T N(E_F)} \right]^{1/4} \quad (6)$$

$$W_{\text{hop}} = \left[\frac{3}{4\pi (R_{\text{hop}})^3 N(E_F)} \right] \quad (7)$$

Therefore, $N(E_F)$, R , and W can be calculated from the observed values of T_0 using Eqs. 5, 6 and 7, after making a proper estimate of L . In the present case L is assumed to be ~ 3 Å, i.e., width on aniline monomer unit. Further the temperature dependence of σ_0 , L , and $N(E_F)$ have been also ignored to simplify the above calculations. The calculated Mott parameters are presented in Table 2.

The data shows that characteristic temperature (T_0) which is a measure of transport resistance, increases with increase in amount of FT. This is again related to the insulating nature of FT phase and consequent obstruction of charge flow. The decrease in $N(E_F)$ is related to the dilution of polaronic concentration. The hopping distance increases and hopping energy decrease in going from FPT1 to FPT2 which may be related to increase in both disorder as well as phonon-assisted hopping probabilities. The Mott's requirement for hopping conduction to nearest neighboring sites can be mathematically represented as $R/L > 1$ and $W_{\text{hop}} > k_B T$ [24–27]. The nanocomposites satisfy the above criteria and justify the applicability of 3D-VRH model in describing their charge transport mechanism. On the other hand, though PANI satisfies the first Mott criteria (i.e. $R/L > 1$) but it just fails to satisfies the second condition (i.e., $W_{\text{hop}} > k_B T$). This may be due to the highly delocalized nature of polarons or fibrous

(rather than particulate) morphology of the PANI. The above fact is also suggested by extremely high value of $N(E_F)$ (i.e., 1.85×10^{23}) which is approaching the theoretical limit, i.e., Avogadro's number (6.023×10^{23}). This could also happen due to concentrated hopping-sites rather than distributed randomly across the samples. The super localization may also lead to erroneous results. However, the above discrepancy is still not fully understood, and our further attempts will try to specifically address and clarify the same with relevant techniques and explanations.

Microwave studies in P-Band (12.4–18 GHz)

Shielding effectiveness measurements have been carried out on a VNA (Agilent E8362B) in the 12.4–18 GHz microwave range. The powder sample has been pressed into a 2.7 mm thick rectangular pellet with a dimension to fit the internal cavity of Ku-band waveguide. The input power level has been kept at 5 dBm. The total EMI SE is the attenuation of ratio of EM (EM) waves produced inside the shield material and can be expressed as [7, 13]:

$$SE_T(\text{dB}) = -10 \log \left| \frac{P_T}{P_I} \right| = -20 \log \left| \frac{E_T}{E_I} \right| = -20 \log \left| \frac{H_T}{H_I} \right| \quad (8)$$

where P_I (E_I) and P_T (E_T) are the incident and transmitted EM powers (electric or magnetic field), respectively. The total SE can further be divided into three components:

$$SE_T = SE_R + SE_A + SE_M \quad (9)$$

where SE_R , SE_A , and SE_M are SE due to reflection, absorption and multiple reflections, respectively. The scattering parameters S_{11} (or S_{22}) and S_{21} (or S_{12}) of a two port network analyzer can be related with reflectance and transmittance as:

$$T = \left| \frac{E_T}{E_I} \right|^2 = |S_{21}|^2 = |S_{12}|^2 \quad (10)$$

and

$$R = \left| \frac{E_R}{E_I} \right|^2 = |S_{11}|^2 = |S_{22}|^2 \quad (11)$$

The absorbance (A) can be written as:

$$A = (1 - R - T) \quad (12)$$

Here, it should be noted that the absorption coefficient is given with respect to the power of the incident EM wave. When SE_A is ≥ 10 dB, SE_M is negligible [28]. Therefore, third term in Eq. 9 (i.e., SE_M) vanishes and SE_T can be conveniently expressed as:

$$SE_T = SE_R + SE_A;$$

The relative intensity of the effectively incident EM wave inside the materials after first reflection is based on the quantity $(1 - R)$. Therefore, the effective absorbance (A_{eff}) can be described as $A_{eff} = (1 - R - T)/(1 - R)$ with respect to the power of the effectively incident EM wave inside the shielding material. Therefore, it is convenient to express the reflection and effective absorption losses in the form of $-10\log(1 - R)$ and $-10\log(1 - A_{eff})$, respectively [26, 29], i.e.

$$SE_R = -10\log(1 - R) \tag{13}$$

$$SE_A = -10\log(1 - A_{eff}) = -10\log\frac{T}{1 - R} \tag{14}$$

The term skin depth (δ) is the depth of penetration at which the intensity of the EM wave is reduced to $1/e$ of its original strength. The δ dependent upon various parameters like angular frequency (ω), real relative permeability (μ') and total conductivity ($\sigma_T = \sigma_{dc} + \sigma_{ac}$), i.e., $\delta = \sqrt{2/\omega\mu\sigma_T}$.

According to EM theory, for electrically thick samples ($t > \delta$), frequency (ω) dependence of far field losses can be expressed in the terms of total conductivity (σ_T), real permeability (μ'), skin depth (δ), and thickness (t) of the shield material.

$$SE_R(\text{dB}) = 10 \log\left(\frac{\sigma_T}{16\omega\epsilon_0\mu'}\right) \tag{15}$$

$$SE_A(\text{dB}) = 20\frac{t}{\delta}\log e = 8.68\left(\frac{t}{\delta}\right) \tag{16}$$

The σ_T and δ can be related to imaginary permittivity (ϵ'') and real permeability (μ') as

$$\sigma_T = \omega\epsilon_0\epsilon'' \tag{17}$$

$$\delta = \left(\frac{2}{\sigma_T\omega\mu'}\right)^{\frac{1}{2}} \tag{18}$$

This gives absorption loss as:

$$SE_A(\text{dB}) = 8.68t\left(\frac{\sigma_T\omega\mu'}{2}\right)^{\frac{1}{2}} \tag{19}$$

Due to shallow skin depths and high conductivity (σ_T) values in the microwave region, contribution of SE_A becomes more as compared to the SE_R . Therefore, absorption acts as dominant shielding mechanism with nominal reflection values. The variation of SE of different samples of PANI-FT composite in the frequency range of 12.4–18 GHz (P-band) is shown in Fig. 7. It has been observed that as we increase the filler in polymer matrix the total SE value increases from 35.64 dB (for FPT1) to 45.20 dB (for FPT2) at 18 GHz which is quite higher than the values obtained using PANI- γ -Fe₂O₃ ($SE_T \sim 11.8$ dB)

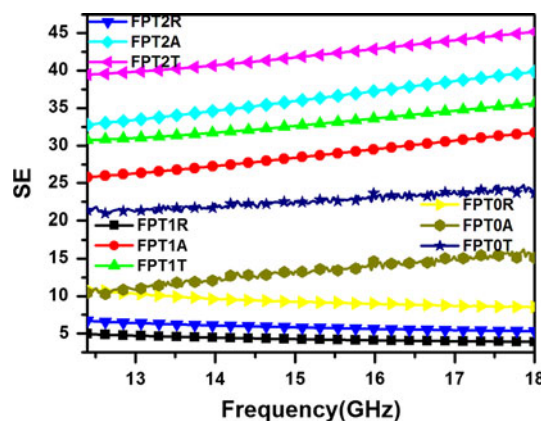


Fig. 7 Dependence of shielding effectiveness (SE_A , SE_R and SE_T) as a function of frequency showing the effect of FT concentration on the SE_A value of PANI-FT composites

and PANI-TiO₂ ($SE_T \sim 25$ dB) composite. As you see from above result that TiO₂ have more significant effect over the Fe₂O₃. The main characteristic feature of TiO₂ is that it has high dielectric constant with dominant dipolar polarization and the associated relaxation phenomenon constitutes the loss mechanism. The values obtained for PANI-FT nanocomposite ($SE_A \sim 39.88$ dB) is lower compare to PANI PTF12 ($SE_A \sim 45$ dB) but as you see from Ref. [16] that the SE_A is higher at 14.6 GHz then there is a dip in the value of SE_A . The reason behind this is the heterogeneity in the PANI-FT composites with difficulty in controlling the EM attributes which lower the effective attenuation of microwave radiations. The other reason behind the greater shielding effective value has been the dense nature of ferrite particle. In our previous work we have used more filler [PANI:TiO₂: γ -Fe₂O₃ :: 1:1:2, i.e., is polymer to filler ratio 1:3] but in this article, we use [PANI:Ti-doped γ -Fe₂O₃ :: 1:2] and achieve nearly same value of SE due to absorption part. To investigate further, we have divided SE_T into two components, i.e., SE_R (due to reflection) and SE_A (due to absorption). The results revealed that though SE_R increases slightly from 3.9 dB (for FPT1) to 5.3 dB (for FPT2) at 18 GHz and SE_A shows rapid enhancement from 31.75 dB (for FPT1) to 39.88 dB (for FPT2) at 18 GHz. To further investigate the reasons behind the observed enhancement in SE and dominance of absorption, the complex permittivity ($\epsilon^* = \epsilon' - i\epsilon''$) and permeability ($\mu^* = \mu' - i\mu''$) have been extracted from experimental scattering parameters (S_{11} and S_{21}) using Nicholson-Ross and Weir expressions [30–32]. The real part or dielectric constant (ϵ') is due to polarization occurring in the material whereas imaginary part (ϵ'') represents dissipated energy. Similarly, the real (μ') and imaginary (μ'') parts of permeability represents magnetization and losses, respectively. The dielectric

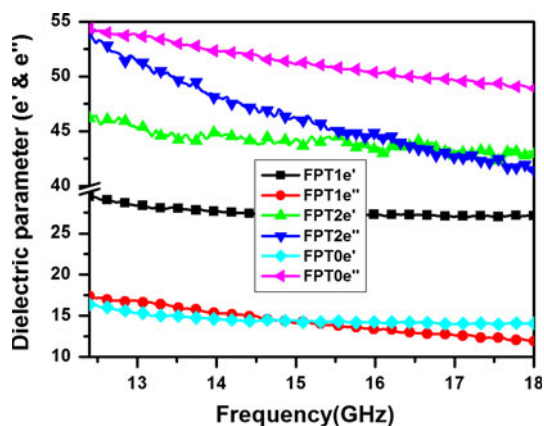


Fig. 8 Behavior of dielectric constant (ϵ') and dielectric loss (ϵ'') of polyaniline–FT composites as a function of frequency

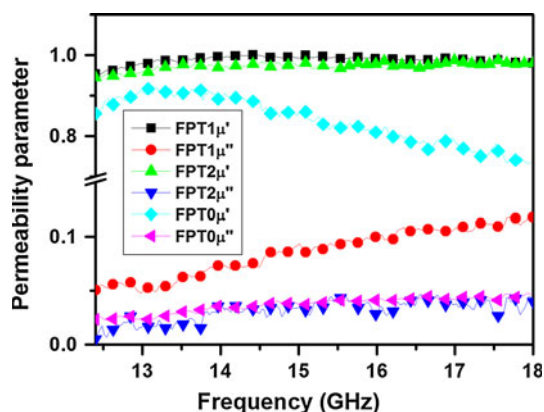
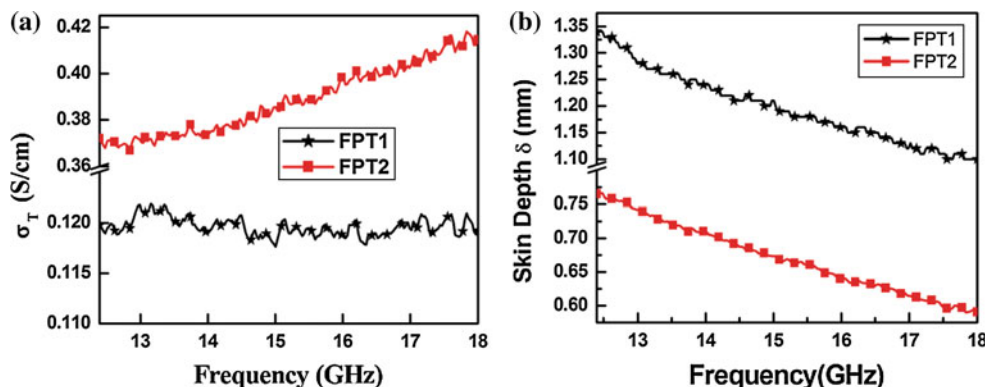


Fig. 9 Behavior of permeability parameter of FPT1, FPT2 as a function of frequency

performance of the material depends on ionic, electronic, orientation, and space charge polarization as well as competing loss mechanisms. On the other hand, hysteresis, domain wall movement, eddy current losses constitute the magnetic losses. In the PANI–FT composites strong space charge polarization occurs due to conductivity

Fig. 10 **a** Variation of total conductivity (σ_T) as a function of frequency. **b** The change in skin depth (δ) with the increase in frequency for the polyaniline–FT composites



difference between PANI and FT phases. Further, the localized charges, i.e., polaron/bipolaron as well as dipoles present in the system account for strong polarization. From Fig. 8, it has been observed that on addition of FT in the polymer matrix, dielectric constant (ϵ') increases from 29 (FPT1) to 46 (FPT2) whereas dielectric loss (ϵ'') increases from 17 (FPT1) to 54 (FPT2). The increase in ϵ' can be attributed to dielectric nature of FT as well as interfacial polarization between PANI and FT. The enhancement of dielectric losses can be attributed to space charge polarization. The super paramagnetic nature of FT nanoparticles imparts additional magnetic property to the nanocomposites. Figure 9 shows that with increase in loading level of FT, μ' remain almost same but the magnetic losses increases from 0.04 to 0.11. According to Eq. 17, imaginary permittivity enhances total conductivity (Fig. 10a), whereas real part of permeability helps in the reduction of skin depth (Fig. 10b). The imaginary permeability is responsible for magnetic losses. The coating of FT nanoparticles with PANI affects the surface electronic charge density, number of dangling bonds and interparticle exchange rates, further contributing toward losses. The increase in FT content leads to reduction of skin depth from 1.1 mm (FPT1) to 0.58 mm (FPT2), enhancement of total conductivity from 0.12 S cm^{-1} (FPT1) to 0.41 S cm^{-1} (FPT2) at 18 GHz along with better matching of input impedance resulting in enhanced SE. The high value (45.20 dB) of absorption dominated SE (>99.99% attenuation) demonstrates the potential of these nanocomposites for making futuristic radar absorbers and efficient microwave shields.

Conclusions

In conclusion, PANI–FT nanocomposites have been successfully synthesised by using in situ emulsion polymerization. Addition of FT (dielectric filler and magnetic filler) in the conducting matrix gave a new kind of composite

materials having better microwave absorption properties ($SE_A \sim 39.88$ dB) which strongly depends on volume fraction of FT in PANI matrix following the 3D-VRH model of charge transport. The presence of FT filler leads to more scattering which in reverse helpful for proper impedance matching and ultimately leads to enhanced absorption of the EM wave.

Acknowledgements Authors wish to thank Director NPL for his keen interest in the work. Authors are also thankful to Dr. Rashmi for XRD patterns, Dr. Renu Pasricha for HRTEM images and Dr. R.K. Kotnala for doing the magnetization measurements of the samples. One of the authors Anoop Kumar S is thankful to UGC for providing junior research fellowship.

References

- Hong YK, Lee CY, Jeong CK, Lee DE, Kim K, Joo J (2003) *Rev Sci Instrum* 74:1098
- Kim HK, Kim MS, Song K, Park YH, Kim SH, Joo J, Lee JY (2003) *Synth Metals* 135:105
- Hoang NH, Wojkiewicz JL, Miane JL, Biscarro RS (2007) *Polym Adv Technol* 18:257
- Wang Y, Jing X (2005) *Polym Adv Technol* 16:344
- Dhawan SK, Singh N, Venkatachalam S (2002) *Synth Metals* 129:261
- Das NC, Yamazaki S, Hikosaka M, Chaki TK, Khastgir D, Chakraborty A (2005) *Polym Int* 54:256
- Singh AP SAK, Chandra A, Dhawan SK (2011) *AIP Adv* 1:022147
- Murugesan R, Subramanian E (2003) *Bull Mater Sci* 26(5):529
- Schnitzler DC, Meruvia MS, Hümmelgen IA, Zarbin AJG (2003) *Chem Mater* 15:4658
- Wan M, Fan J (1998) *J Polym Sci* 36:2749
- Xuan SH, Wang YXJ, Leung KCF, Shu KY (2008) *J Phys Chem C* 112:18804
- Ohlan A, Singh K, Chandra A, Dhawan SK (2008) *Appl Phys Lett* 93:053114
- Ohlan A, Singh K, Chandra A, Singh VN, Dhawan SK (2009) *J Appl Phys* 106:044305
- Singh K, Ohlan A, Kotnala RK, Bakhshi AK, Dhawan SK (2008) *Mater Chem Phys* 112:651
- Dhawan SK, Singh K, Bakhshi AK (2009) *Synth Metals* 159(21–22): 2259
- Singh K, Ohlan A, Bakhshi AK, Dhawan SK (2010) *Mater Chem Phys* 119:201
- Cornell RM, Schertmann U (2000) *Iron oxides in the laboratory preparation and characterization*, 2nd edn. Wiley, New York
- Jiang J, Li L, Xu F (2007) *J Appl Polym Sci* 105:944
- Yakuphanoglu F, Basaran E, Suenkal BF, Sezer E (2006) *J Phys Chem B* 110:16908
- Mott NF, Davis EA (1979) *Electronic processes in noncrystalline materials*, 2nd edn. Oxford University Press, New York
- Sanjai B, Raghunath A, Natrajan TS, Rangarajan GS, Thomas PVP, Venkatachalam S (1997) *Phys Rev B* 55:10734
- Singh R, Narula AK, Tandon RP, Mansingh A, Chandra S (1996) *J Appl Phys* 79:1476
- Lee CY, Song HG, Jang JS, Oh EJ, Epstein AJ, Joo J (1999) *Synth Metals* 102:1346
- Singh K, Ohlan A, Saini P, Dhawan SK (2008) *Polym Adv Technol* 19:229
- Li J, Fang K, Qiu H, Li S, Mao W (2004) *Synth Metals* 142:107
- Pinto NJ, Kahol PK, McCormick BJ, Dalal NS, Han H (1994) *Phys Rev B* 49:13983
- Reghu M, Cao Y, Moses D, Heeger A (1993) *J Phys Rev B* 47:1758
- Das NC, Khastgir D, Chaki TK, Chakraborty A (2000) *Compos A* 31:1069
- Colaneri NF, Shacklette LW (1992) *IEEE Trans Instrum Meas* 41:291
- Nicolson AM, Ross GF (1970) *IEEE Trans Instrum Meas* 19:377
- Weir WB (1974) *Proc IEEE* 62:33
- Phang SW, Hino T, Abdullah MH, Karamoto N (2007) *Mater Chem Phys* 104:327